CORROSION SCIENCE AND TECHNOLOGY, Vol.4, No.5(2005), pp.178~190

A Galvanic Sensor for Monitoring the External and Internal Corrosion Damage of Buried Pipelines

†Yoon-Seok Choi[1], Jung-Gu Kim[1], and Woon-Suk Hwang[2]

[1]Dept. of Advanced Materials Engineering, Sungkyunkwan University
300 Chunchun-Dong, Jangan-Gu, Suwon 440-746, KOREA
[2]School of Meterials Science and Engineering, Inha University
253 Yonghyun-Dong, Nam-Gu, Incheon, 452-751, KOREA

In order to develop a new corrosion sensor for detecting and monitoring the external and internal corrosion damage of buried pipeline, the electrochemical property of sensors and the correlation of its output to corrosion rate of steel pipe, were evaluated by electrochemical methods in two soils of varying resistivity (5,000 ohm-cm, 10,000 ohm-cm) and synthetic tap water environments. In this paper, two types of galvanic probes were manufactured: copper-pipeline steel (Cu-CS) and stainless steel-pipeline steel (SS-CS). The corrosion behavior in synthetic groundwater and synthetic tap water for the different electrodes was investigated by potentiodynamic test. The comparison of the sensor output and corrosion rates revealed that a linear relationship was found between the probe current and the corrosion rates. In the soil resistivity of 5,000 Ω-cm and tap water environments, only the Cu-CS probe had a good linear quantitative relationship between the sensor output current and the corrosion rate of pipeline steel. In the case of 10,000 Ω-cm, although the SS-CS probe showed a better linear correlation than that of Cu-CS probe, the Cu-CS probe is more suitable than SS-CS probe due to the high current output.

Keywords : *galvanic sensor, corrosion monitoring system, pipeline, galvanic currents, soil environment, tap water environment*

1. Introduction

For many years, frequent replacement of corroded pipelines was an unchallenged cost where aggressive soil conditions promoted extensive external corrosion.[1)] External corrosion of water distribution systems leads to two major problems for water utilities. The first problem is the failure of the distribution system pipes. The second is the contamination of water as the contaminants in soil are transported into the distribution system.[2)] Although the internal corrosion rate of steel is small in potable water distribution systems, internal corrosion in distribution systems for potable water causes considerable expense for the municipalities.[3-5)] The consequences of internal corrosion are pipe breaks, overflow, clogging of pipes with corrosion products and, the most important problem is water quality deterioration. Corrosion products containing metal ions are found at the consumers' taps as well as at the sewage treatment plant, degrading the quality of the sludge that may be used as a soil improver. In addition, polluted potable water can cause health problems.

To protect against external and internal corrosion, a number of methods including coatings, cathodic protection, coal-tar lining and cleaning were used.[6,7)] These methods can reduce effectively the corrosion damage in potable water pipeline, but it is a cost problem due to additional equipments for installation. Moreover, corrosion problems still can occur on the system under certain conditions. Therefore, it has become urgent to have reliable sensor systems for accurately measuring the rate of corrosion in existing as well as new structures and for evaluating the corrosion protection provided by various treatments.

A variety of electrochemical techniques are now being widely employed for monitoring the corrosion damage of structures.[8-10)] However, the advantages and disadvantages of each respective method have not led to an unambiguous test method. For example, open-circuit potential measurements are rapid and simple, but the measurements provide no information on the kinetics of the corrosion process.[11)] Linear polarization tests are also relatively simple but require compensation of the high ohmic resistance of

†Corresponding author: kimjg@skku.ac.kr

electrolyte.[12] The obstacle of ohmic compensation can be overcome with electrochemical impedance spectroscopy (EIS). While EIS can provide precise information on corrosion rates, diffusion processes and material heterogeneities can create spectra that are extremely difficult and time-consuming to interpret.[13]

Galvanic probe corrosion monitors are simple, rugged instruments constructed of two dissimilar metals that are submerged in the electrolyte to be studied. The direct current generated by the dissimilar metals is a function of the corrosiveness of the electrolyte in which the probe is submerged. Other than corrosion coupons, galvanic probes are among the least complicated of all corrosion monitors. The probes reflect changes in corrosion conditions very rapidly, usually within a few minutes.[14-16] Thus, galvanic probes have been successfully used in concrete structures[17-20] and aircrafts.[15,21] However, in the field of buried structures, there is only limited success in detecting the changes in the system, e.g., temperature, pH, oxygen content, salinity, or conductivity, which results in a change in the current output of the probe.[9,14] Thus, the galvanic sensor system developed until now, can not supply the quantitative corrosion rate of pipeline, but only provide the information of the presence of corrosion.

The sensor was developed using well known principles of galvanic corrosion.[15,21] When two dissimilar elements of the galvanic sensor are exposed to an environment but kept isolated from each other, they corrode at their respective corrosion rates. But when they are electrically connected together, they become galvanically coupled. A galvanic current is developed when an electrolyte from the environment bridges the gap between the two electrodes. A zero resistance ammeter (or a potentiostat acting as a ZRA) was used to short-circuit the electrode such that galvanic current can be measured using a high impedance voltmeter interposed between the electrodes. The magnitude of this galvanic current is directly proportional to the corrosivity of the soil and the corrosion rate of the pipeline steel. Fig. 1 illustrates the operation of galvanic sensor system developed in this study.

The objective of this study is to present the results of evaluations of the ability of galvanic sensor system to detect the real world corrosion damage in various environments, and to determine the reliable cathode materials for galvanic sensor system by electrochemical experiments in laboratory.

2. Experimental

2.1 Sensor system

Steel specimens were cut from an API Grade A (STWW 400) carbon steel (CS) pipeline. Materials for the cathode in sensor system were selected from conventional type 304 stainless steel (SS) and pure copper (Cu). Table 1 lists the chemical compositions of pipeline steel (anode) and more noble metals (cathode), respectively. The specimens were machined in the shape of a bar with a diameter of 12 mm and a height of 50 mm, and ground with 120 grit silicon carbide paper and finished with 600 grit paper.

Using the anode and cathode materials shown in Table

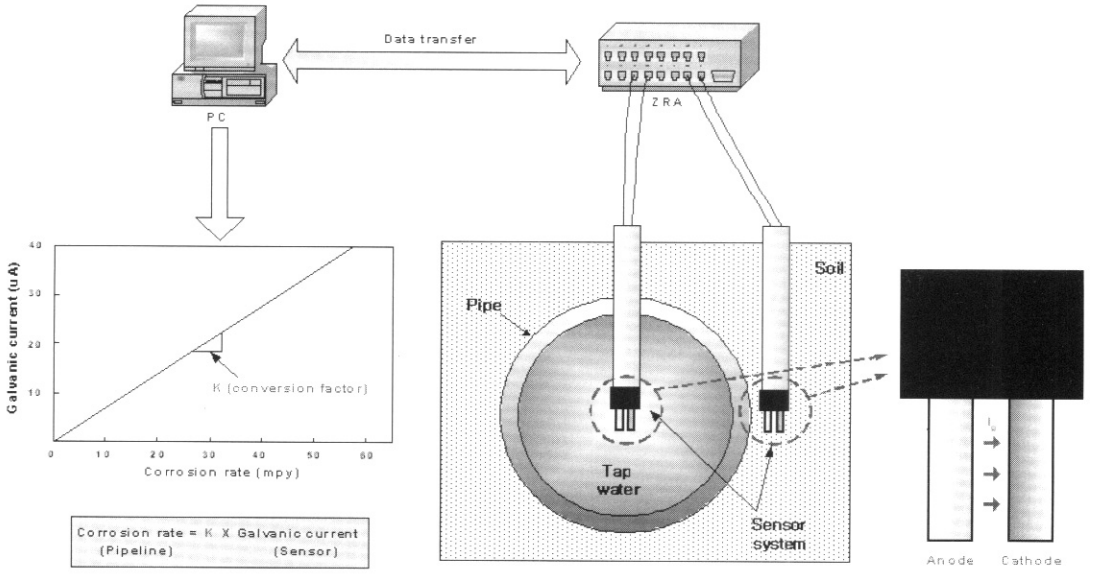

Fig. 1. Schematic illustration of operation of galvanic sensor system.

Table 1. Chemical compositions of sensor elements (wt. %)

	C	Mn	P	S	Si	Cr	Ni	Cu	Fe
CS (STWW 400)	0.25	-	0.04	0.04	-	-	-	-	bal
SS (AISI 304)	0.08	2.0	0.045	0.03	1.0	18.2	8.2	-	bal
Cu	-	-	-	-	-	-	-	99.99	-

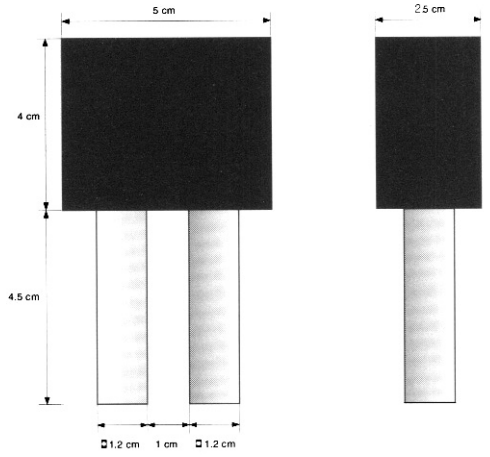

Fig. 2. Galvanic probe sensor consisting of a pipeline steel and noble metal cathode.

1, the Cu-CS and SS-CS galvanic sensors were manufactured as shown in Fig. 2. The anode and cathode were machined in the shape of a bar with a diameter of 12 mm, a height of 45 mm, and the distance between anode and cathode was 10 mm.

2.2 Environments

Groundwater, soil and tap water samplings were conducted on the representative sites where the pipelines were buried. The samples were analyzed using several quantitative analytical techniques to prepare the test solution.[22,23] Table 2 and 3 give the chemical composition of the synthetic groundwater and synthetic tap water, which is based on the average contents of samples collected from the field.

Table 2. Chemical composition of synthetic groundwater

Calcium chloride ($CaCl_2$)	133.2 mg/L
Magnesium sulfate ($MgSO_4 \cdot 7H_2O$)	59 mg/L
Sodium bicarbonate ($NaHCO_3$)	208 mg/L
Sulfuric acid (H_2SO_4) (97 wt. %)	48 mg/L
Nitric acid (HNO_3) (70 wt. %)	21.77 mg/L
pH	6.76
Resistivity	1.736 kΩ-cm

Table 3. Chemical composition of synthetic tap water

Total hardness (as Ca^{2+} and Mg^{2+})	46.3 mg/L
SO_4^{2-}	24.33 mg/L
Cl^-	16.96 mg/L
pH	7.4
Resistivity	3.533 kΩ-cm

2.3 Polarization test

Electrochemical polarization of the sensor elements was accomplished with an EG&G Model 273A potentiostat. The potentiostat was programmed to apply a continuously varying potential to the sample at a rate of 600 mV/h. Each specimen was mounted in epoxy that was cured in an air for 24h. The specimen was finished by grinding on 600-grit silicon carbide paper. To prevent the initiation of crevice corrosion between the epoxy and the specimen, the epoxy-specimen interface was painted with Amercoat 90 epoxy, leaving an exposed area of 1 cm^2 on the material surface. All potentials were measured against the saturated calomel electrode (SCE). For each material and electrolyte combination, the corrosion sample was allowed to stabilize in the electrolyte, until the potential change was < 1 mV/min. This potential then was taken as the open-circuit potential (OCP). To insure reproducibility, at least three replicates were run for each specimen. The polarization tests were performed in the stagnant synthetic groundwater under ambient laboratory condition.

Corrosion rates were determined by Tafel extrapolation method. The corrosion current density can be measured and can yield a corrosion rate, based on Faraday's law:[24]

$$\text{Corrosion rate (mpy)} = \frac{0.13 \times i_{corr}(\text{uA/cm}^2) \times \text{E.W.}}{\text{density(g/cm}^3)} \quad (1)$$

where mpy is mils per year, 0.13 is the metric and time conversion factor and, E.W. is the equivalent weight in grams.

2.4 Soil and tap water test cell

To evaluate the correlation between sensor output and corrosion rate of pipeline steel in soil environments and synthetic tap water, the probes were placed in soil chambers with different soil resistivities (5,000 Ω-cm, 10,000 Ω-cm), and in tap water chamber. Also, the pipeline steel was placed in the middle of each chamber with two graphite counter electrodes and a copper/copper sulfate ($Cu/CuSO_4$) reference electrode, to measure the corrosion rate of pipeline steel. The arrangements of test cells are illustrated in Fig. 3.

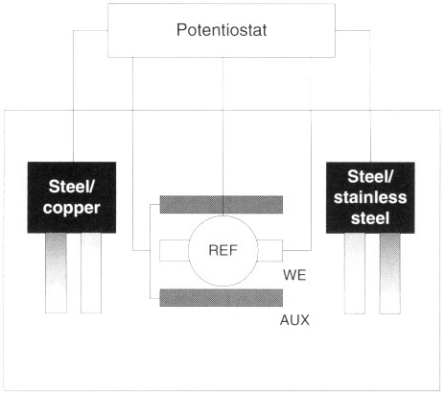

(a)

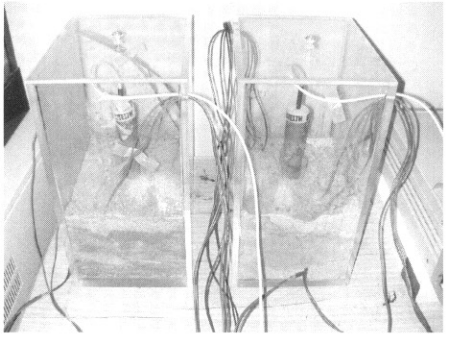

(b)

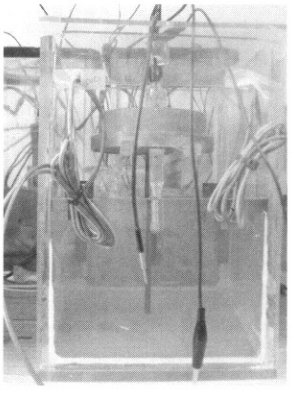

(c)

Fig. 3. Experimental setup of galvanic sensor system for electrochemical measurements: (a) arrangement of sensor and electrodes, (b) soil test cell, (c) tap water test cell.

Unlike the water, the soil presents a highly heterogeneous structure. Clays may have a resistivity below 1,000 Ω-cm, while clean gravel will have over 100,000 Ω-cm resistivity.[8] In the present study, with reference to an approximate relationship between soil resitivity and soil corrosivity,[9] two values of soil resistivity were selected as moderate (5,000 Ω-cm) and slight (10,000 Ω-cm) corrosive conditions. The soil resistivity of test chamber was adjusted using synthetic groundwater, and measured by the 4-pin Wenner technique, in which portable instrumentation applies an alternating current, between two outer pin contacts in the soil and induces a potential drop, between two inner pin contacts.

2.5 Galvanic corrosion test

Galvanic corrosion tests were performed using a zero resistance ammeter to measure the output (current) of Cu-CS and SS-CS probes in each environment. The galvanic current was measured for 30 minutes every 10 days in soil environments and 5 days in synthetic tap water. The averages of the measuring values were taken after their stabilization within the range of stabilized current.

2.6 Linear polarization resistance (LPR) and electrochemical impedance spectroscopy (EIS) measurements

The corrosion rates of pipeline steel in each test chamber were measured every 5 or 10 days by LPR and EIS measurements to compare with the integrated probe current to find out the relation between the actual corrosion rate and the sensor output.

LPR measurements were performed within ±20 mV with respect to the corrosion potential with a scan rate of 0.166 mV/s. EIS measurements were conducted in the frequency range between 10 kHz and 10 mHz. Sinusoidal voltage of ±10 mV was supplied and DC potential was set to corrosion potential.

3. Results and discussion

3.1 Electrochemical properties of sensor elements

Figs. 4 and 5 illustrate the polarization curves of sensor elements in synthetic groundwater and synthetic tap water. Carbon steel and copper exhibited active corrosion behavior, whereas stainless steel demonstrated spontaneous

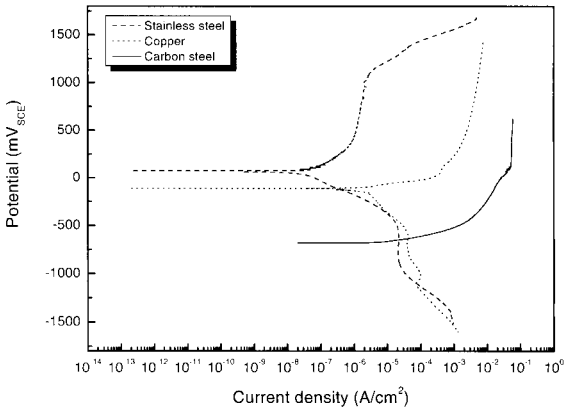

Fig. 4. Polarization curves of sensor elements in synthetic groundwater.

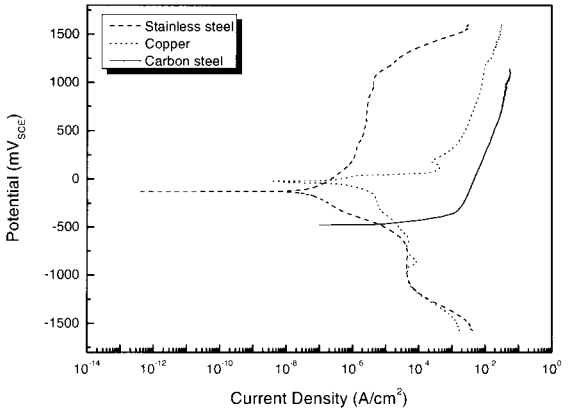

Fig. 5. Polarization curves of sensor elements in synthetic tap water.

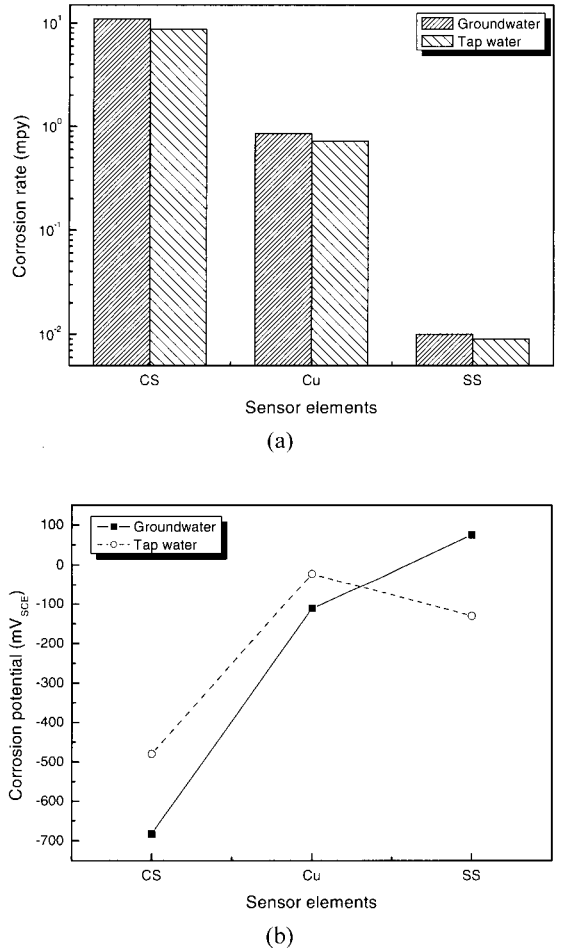

Fig. 6. Corrosion rate (a) and corrosion potential (b) of sensor elements in synthetic groundwater and tap water.

passivation in both environments.

Fig. 6 shows the corrosion rate and corrosion potential of sensor elements in synthetic groundwater and tap water, measured by the Tafel extrapolation method. As shown, sensor elements in groundwater had higher corrosion rates than in tap water, indicates the corrosion property of sensor elements correlates to the corrosivity of the electrolyte.

It is important to note that the current generated by sensor elements selected in this study is of sufficient magnitude to detect the changes in electrolyte. Thus the galvanic effect between sensor elements was predicted using polarization curves. The prediction for the galvanic corrosion of metals is simply the superposition of all of the relevant polarization curves.[25] This can be accomplished by graphically superimposing these curves. In the polarization curves shown in Figs. 4 and 5, the intersection of anodic curve and cathodic curve indicates the predicted galvanic current density (i_g) and potential (E_g) in each environment. Table 2 represents the predicted i_g and E_g in synthetic groundwater and tap water. The predicted i_g was much higher in groundwater than in tap water for Cu-CS and SS-CS couples, indicated the possibility of detecting a difference of the corrosivity of environments by measuring the galvanic current between sensor elements. In addition, Cu-CS couple had a higher i_g than SS-CS couple, implied that the Cu-CS design is more sensitive to corrosive conditions due to the active corrosion behavior of copper.

It is often assumed that the rate of galvanic corrosion can be judged based on the difference of the corrosion potential of uncoupled dissimilar metals.[26,27] From the results of polarization test, it can be expected that the galvanic effect in synthetic groundwater is higher in SS-CS couple because the driving force or difference between anode and cathode potentials is higher than in Cu-CS couple. However, as shown in Table 4, the predicted galvanic current of Cu-CS couple was higher than that of SS-CS couple. This behavior can be explained by the cathodic reaction of cathode materials. For diffusion-controlled cathodic process, the dissolution rate of the anode in a galvanic couple should be independent of the nature of the cathode and therefore also independent of the potential difference between anode and cathode.[28] Fig. 7 shows the superposition of cathodic polarization curves of cathodes and anodic polarization curve of anode in synthetic groundwater. The anodic curve was laid on the oxygen diffusion process region of cathodic curves. The

Table 4. Predicted galvanic current density (i_g) and potential (E_g) in synthetic groundwater and tap water

	Groundwater		Tap water	
	i_g (uA/cm^2)	E_g (mV)	i_g (uA/cm^2)	E_g (mV)
Cu-CS	42.8	-634	19.4	-453
SS-CS	21.4	-648	5.8	-467

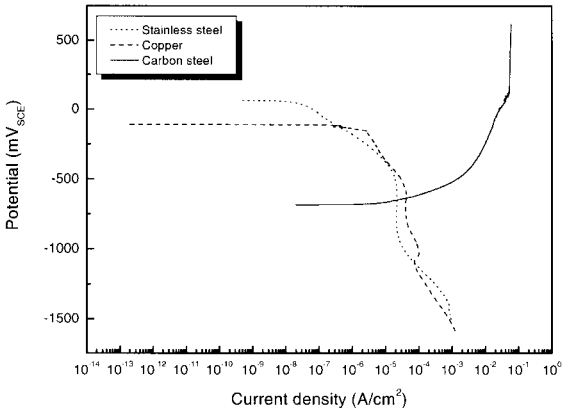

Fig. 7. Cathodic polarization curves of cathodes and anodic polarization curve of anode in synthetic groundwater.

limiting diffusion current density was dependent on the formation of surface films which change the ratio of D/δ in following equation:[29]

$$i_L = \frac{nFDC_{O_2}}{\delta} \quad (2)$$

where n is the number of electrons participating in the reaction, F is the Faraday constant, D is the diffusion coefficient of oxygen, C_{O2} is the oxygen concentration in the bulk solution and δ is the thickness of the diffusion layer. Due to this fact, in this case, the rate of galvanic corrosion depends on not the potential difference between anode and cathode, but the cathodic process of the cathodes.

3.2 Galvanic current measurements for galvanic sensor

Figs. 8 and 9 show the results of prolonged exposure tests of the Cu-CS and SS-CS probes with soil environments and synthetic tap water. The galvanic currents are appreciably higher when carbon steel is coupled to copper than when it is coupled to stainless steel, regardless of measuring environments. However, there is some distinction in the variation of galvanic current with environments in each probe.

The output of Cu-CS probe varied in the range of 8 to 20 uA/cm^2 (144 to 360 uA), whereas the galvanic current of SS-CS probe slowly drifted to lower values of ~ 1 uA/cm^2 (18 uA) with time in soil cell 1 (5,000 Ω-cm). In the case of soil cell 2 (10,000 Ω-cm), the galvanic currents of Cu-CS and SS-CS probes decreased with increasing time, and both probes varied in order of nA/cm^2 scale. This indicated that the soil resistivity of 10,000 Ω-cm was less corrosive condition to change the electrochemical reactions of anode and cathode materials, thus the Cu-CS and SS-CS probes showed similar behavior of

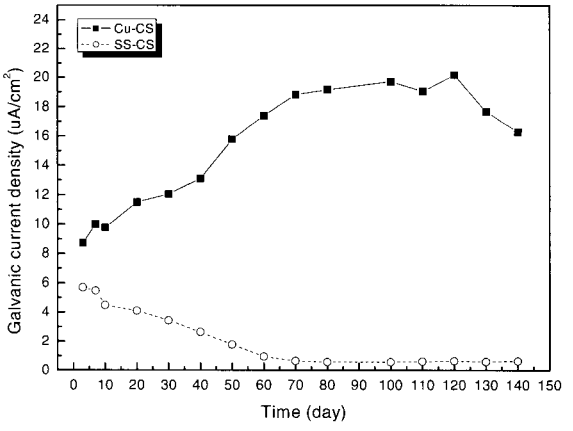

(a)

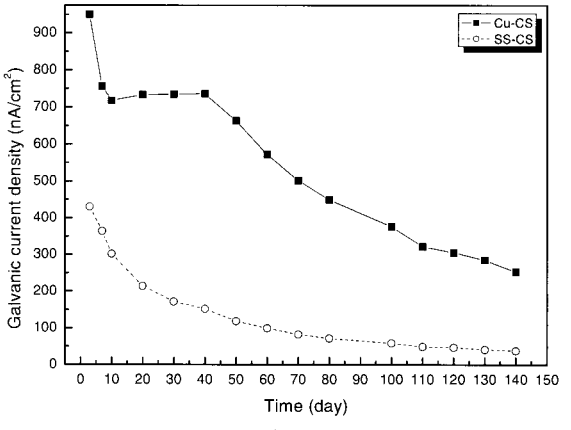

(b)

Fig. 8. Results of the galvanic current measurements for the Cu-CS and SS-CS probes: (a) soil cell 1 (5,000 Ω-cm) and (b) soil cell 2 (10,000 Ω-cm).

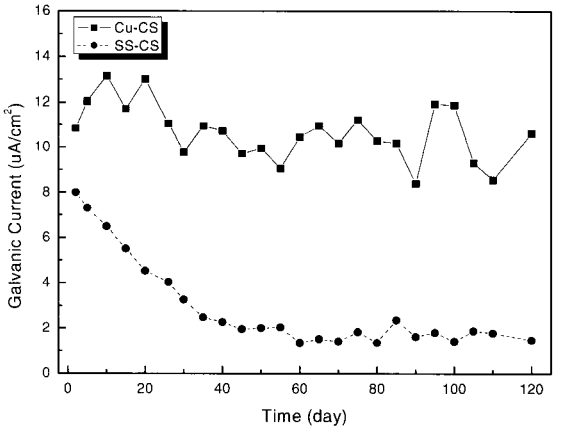

Fig. 9. Results of the galvanic current measurements for the Cu-CS and SS-CS probes in synthetic tap water.

sensor output. In tap water cell, the output of Cu-CS probe varied in the range of 8.3 to 13.2 uA/cm^2 (149.4 to 237.6 uA), whereas the galvanic current of SS-CS probe showed

similar behavior with soil cell 1.

From the results of galvanic current measurements, it is interesting to note that the galvanic currents of SS-CS probe stabilized below 1 uA/cm^2 in all test environments. This behavior was related to the passivation of stainless steel cathode. Stainless steel surface maintains passive film; this apparently causes the low sensor output.

3.3 Corrosion rate measurements for pipeline steel

Corrosion rates of pipeline steel in test chambers were measured by LPR and EIS measurements. Using the polarization resistance (R_p) obtained from LPR and EIS measurements, the corrosion current density (i_{corr}) can be calculated by the following equation, and this i_{corr} yields the corrosion rate using equation (1):

$$i_{corr} = \frac{\beta_{ox,M} \times \beta_{red,C}}{2.3 \times R_p \times (\beta_{ox,M} + \beta_{red,C})} \quad (3)$$

where $\beta_{ox,M}$ is the anodic Tafel constant in mV/decade, $\beta_{red,C}$ is the cathodic Tafel constant in mV/decade.

Fig. 10 shows the variation of corrosion rate measured by LPR measurements with different environments. Initially, the corrosion rate of soil cell 1 rose gradually, and then it slightly decreased after 110 days. However, in the case of soil cell 2, the corrosion rate decreased with increasing test time and maintained very low values less than 0.5 mpy, indicating the specimen was slightly damaged by corrosion reaction. In tap water cell, the corrosion rate of pipeline steel varied in the range of 2.8 to 4.5 mpy.

The Nyquist plots of the pipeline steel with different environments are shown in Figs. 11 and 12. The impedance spectra measured in soil cell 1 represented initially one time constant, changing to two-time constant.

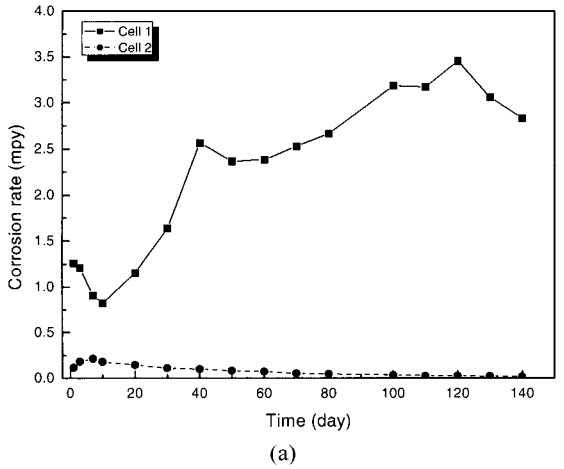

Fig. 10. Variation of corrosion rates measured by LPR measurements with different environments: (a) soil environments, (b) synthetic tap water.

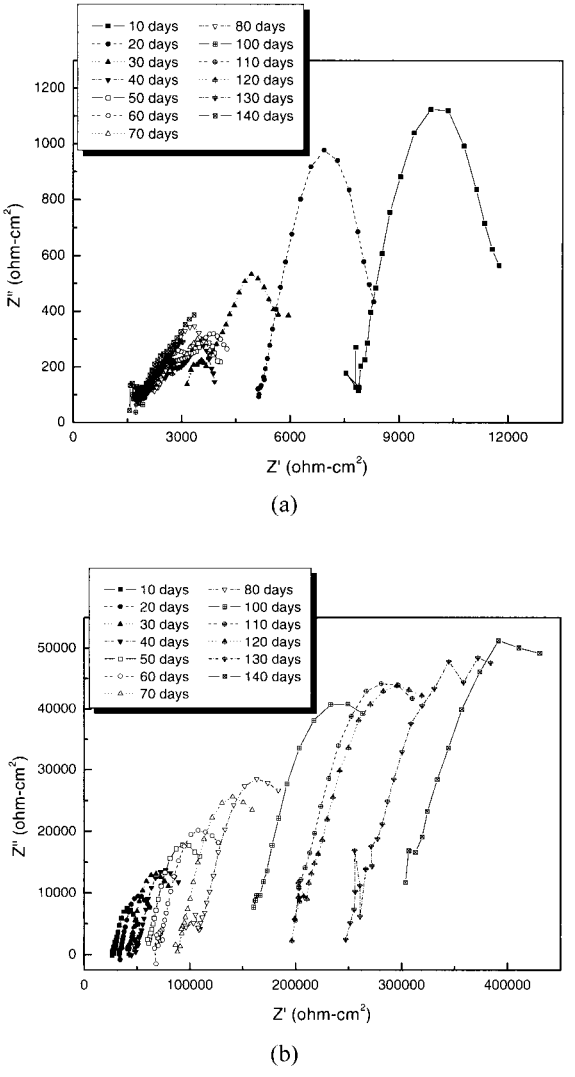

Fig. 11. Nyquist plots for pipeline steel in soil environments: (a) cell 1 and (b) cell 2.

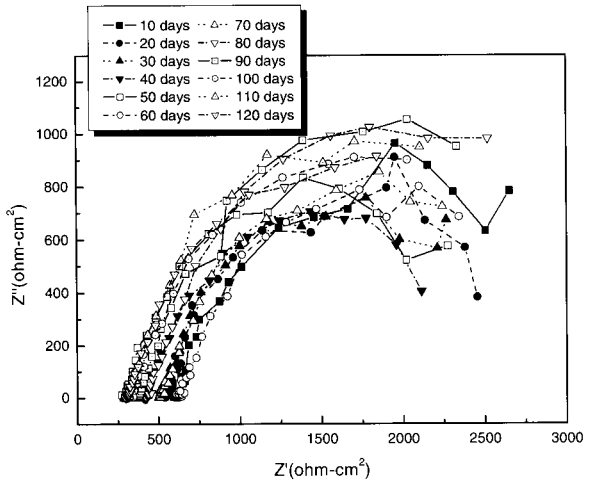

Fig. 12. Nyquist plots for pipeline steel in synthetic tap water.

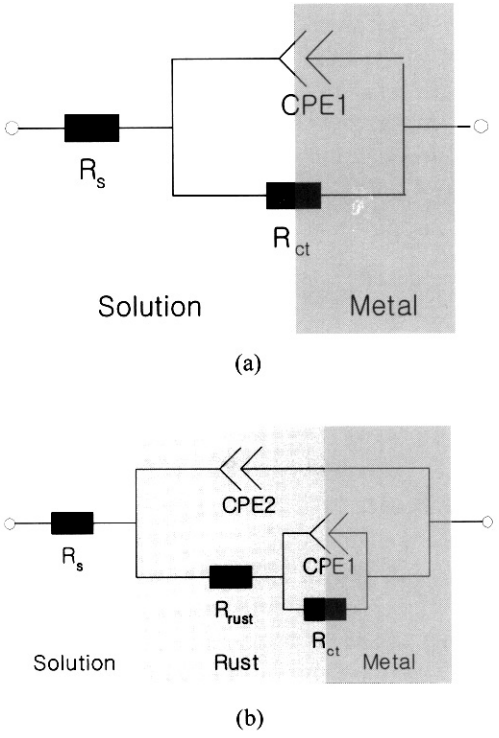

Fig. 13. Equivalent circuits for EIS data fitting: (a) Case for one time constant and (b) Case for two-time constant.

This result is caused by the formation of rust layer, which reacts electrochemically with electrolyte. Also it can be found that the plot was shifted to left with time, indicating decreased solution resistance (R_s). However, in soil cell 2 and tap water cell, the Nyquist plot showed one time constant.

The equivalent circuits represented in Fig. 13 were applied to model the EIS data for specimens and enabled the parameter values for the individual elements to be determined with a least-squares analysis. The optimized values for the resistance parameters are shown in Fig. 14 for soil cell 1 and soil cell 2, and Fig. 15 for tap water cell.

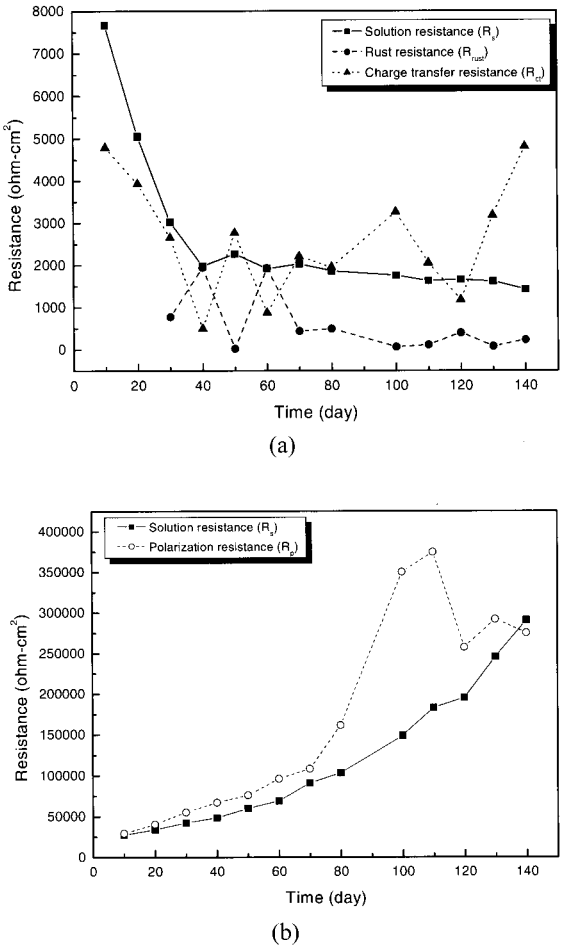

Fig. 14. Resistance parameters as a function of time in soil environments: (a) cell 1 and (b) cell 2.

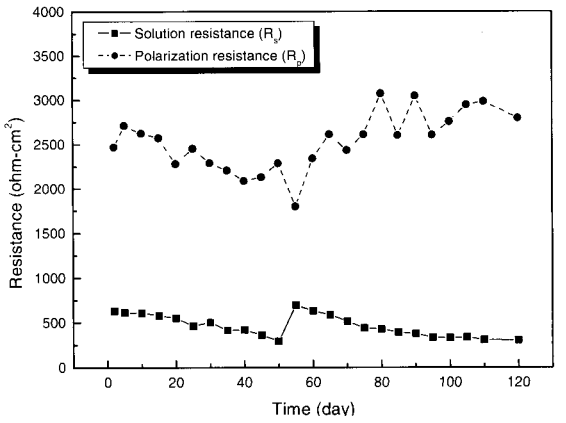

Fig. 15. Resistance parameters as a function of time in synthetic tap water.

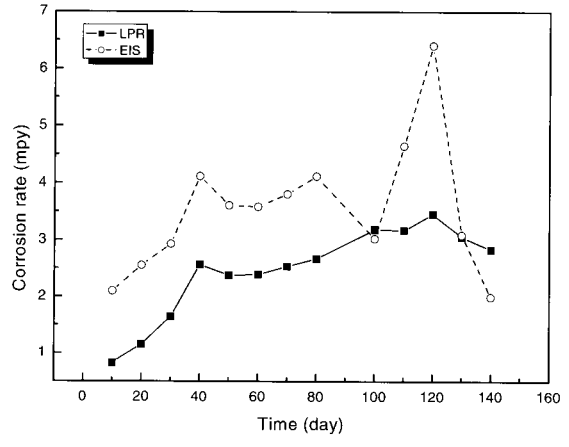

(a)

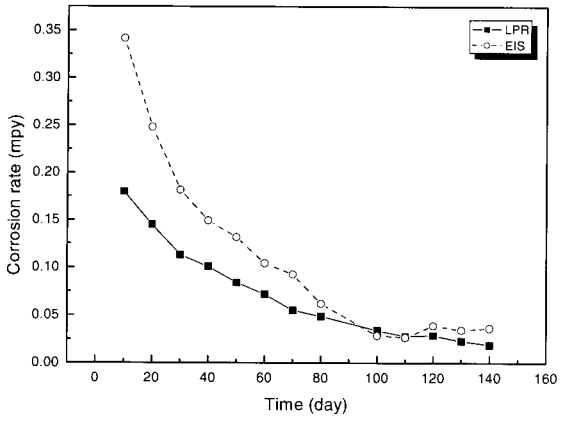

(b)

Fig. 16. Relationship of corrosion rate between LPR and EIS measurements in soil environments: (a) cell 1 and (b) cell 2.

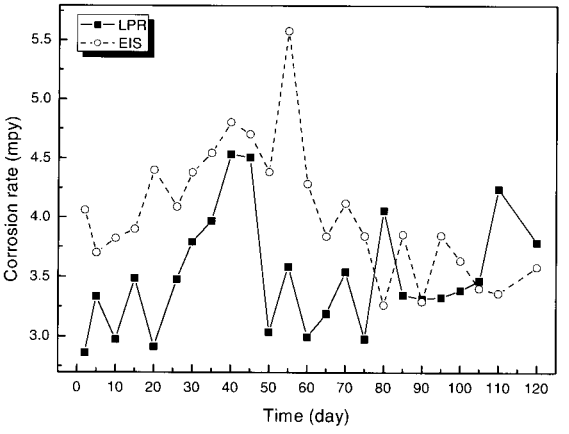

Fig. 17. Relationship of corrosion rate between LPR and EIS measurements in synthetic tap water.

Figs. 16 and 17 represent an attempt that was made to correlate the corrosion rates of pipeline steel obtained by LPR and EIS measurements as a function of time. EIS measurement show higher values because the R_p from EIS measurement compensated for the solution resistance (R_s).[30] A good correlation was obtained between corrosion rates in both soil cells and tap water cell. From this result, it was suggested that the corrosion rates obtained by these methods are suitable for using the evaluation of the correlation with sensor output in soil environments and synthetic tap water.

3.4 Correlation of probe current to actual corrosion rate

To investigate the possibility that galvanic currents can be used to determine the instantaneous corrosion rate of buried pipeline, the cumulative charge of pipeline steel was compared to the galvanic probe output. Electrochemical reactions either produce or consume electrons. Thus, the rate of electron flow to or from a reacting interface is a measure of reaction rate. Electron flow is conveniently measured as current, I, in amperes, where 1-ampere is equal to 1-coulomb of charge (6.2 X 10^{18} electrons) per second. The galvanic current (I_g) and time (t) were integrated to get the coulombic value (Q) based on Faraday's law:[29]

$$Q = I_g \times t \tag{4}$$

From this equation, the total charge of sensor output is used for a comparison with the total charge of pipeline steel obtained by LPR and EIS measurements.

Soil cell 1 (5,000 Ω-cm): Figs. 18 and 19 present the correlation between the coulomb values of the galvanic sensor and the pipeline steel obtained from LPR and EIS measurement in soil cell 1. The output of Cu-CS probe showed a better linear correlation than that of SS-CS probe. Thus, it can be suggested that the Cu-CS sensor system is better reliable in the soil resistivity of 5,000 Ω-cm (moderate corrosive condition).

Soil cell 2 (10,000 Ω-cm): Figs. 20 and 21 illustrate the correlation between the coulomb values of the galvanic sensor and the pipeline steel obtained from LPR and EIS measurement in soil cell 2. A good correlation was observed in the two probes. Contrary to the result in soil cell 1, the SS-CS probe showed a more reliable linear relationship between real corrosion rate and sensor output than the Cu-CS probe. However, the Cu-CS probe is more suitable for high resistance soil than SS-CS probe, due to the high current output.

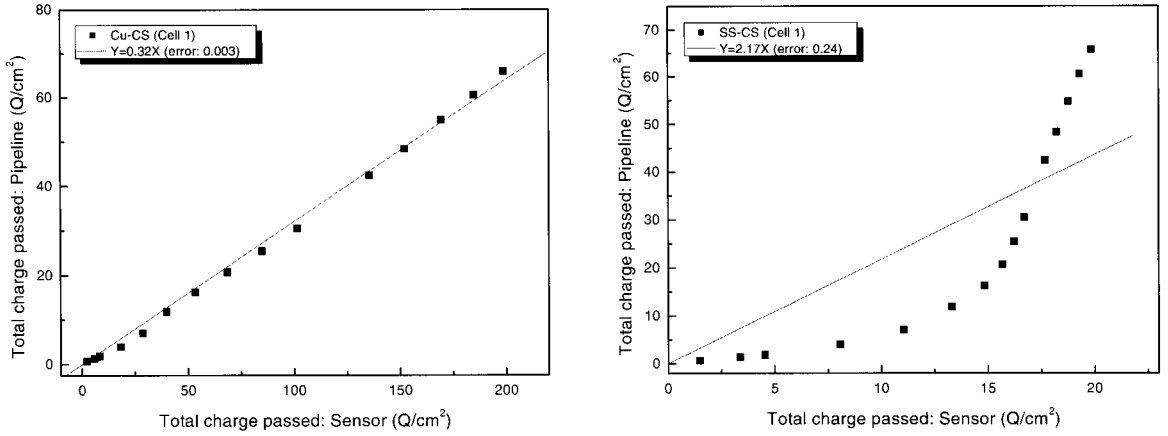

(a) (b)

Fig. 18. The relationship between the cumulative charges of pipeline steel obtained from LPR measurement and sensor output in soil cell 1: (a) Cu-CS probe and (b) SS-CS probe.

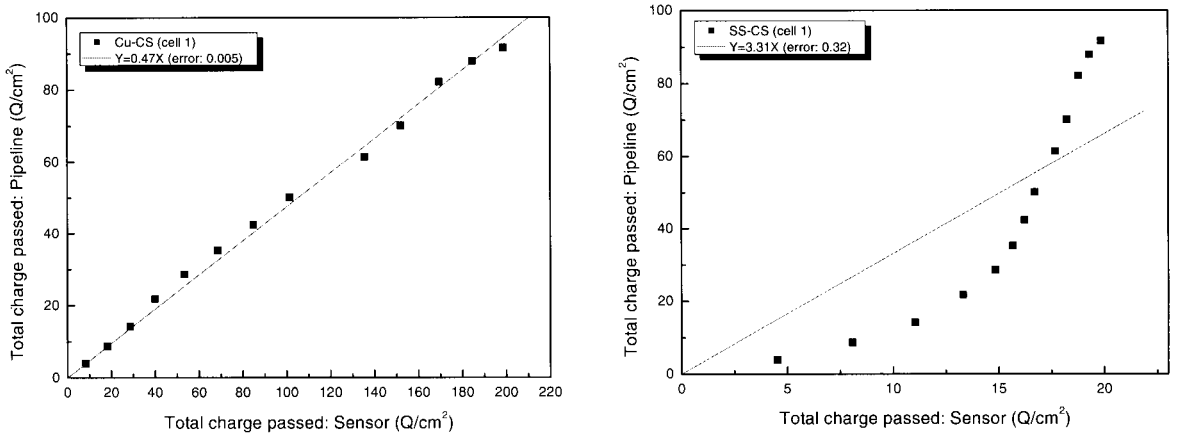

(a) (b)

Fig. 19. The relationship between the cumulative charges of pipeline steel obtained from EIS measurement and sensor output in soil cell 1: (a) Cu-CS probe and (b) SS-CS probe.

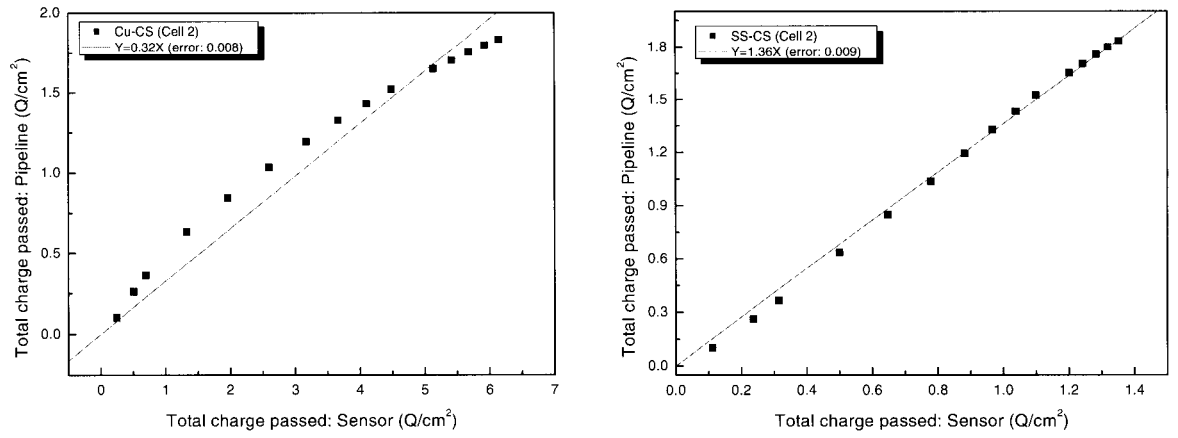

(a) (b)

Fig. 20. The relationship between the cumulative charges of pipeline steel obtained from LPR measurement and sensor output in soil cell 2: (a) Cu-CS probe and (b) SS-CS probe.

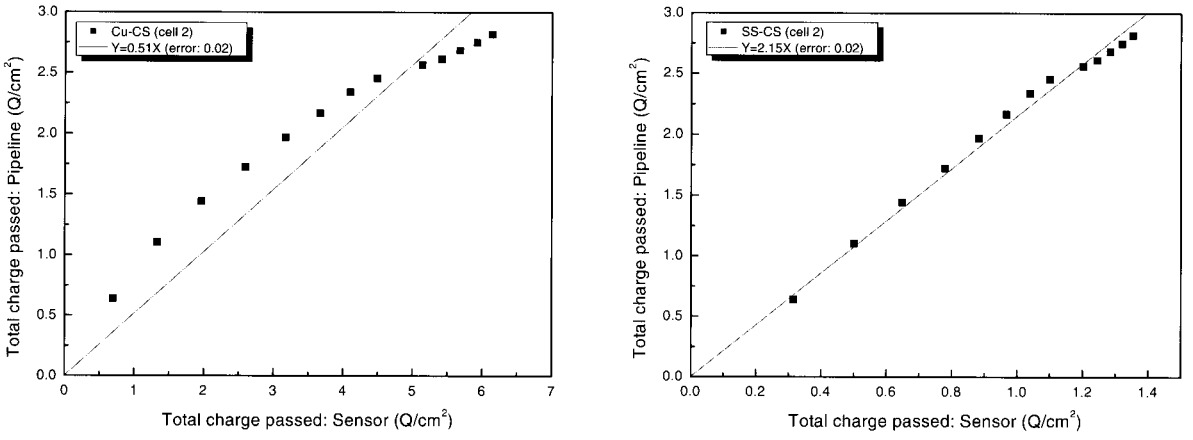

(a) (b)

Fig. 21. The relationship between the cumulative charges of pipeline steel obtained from EIS measurement and sensor output in soil cell 2: (a) Cu-CS probe and (b) SS-CS probe.

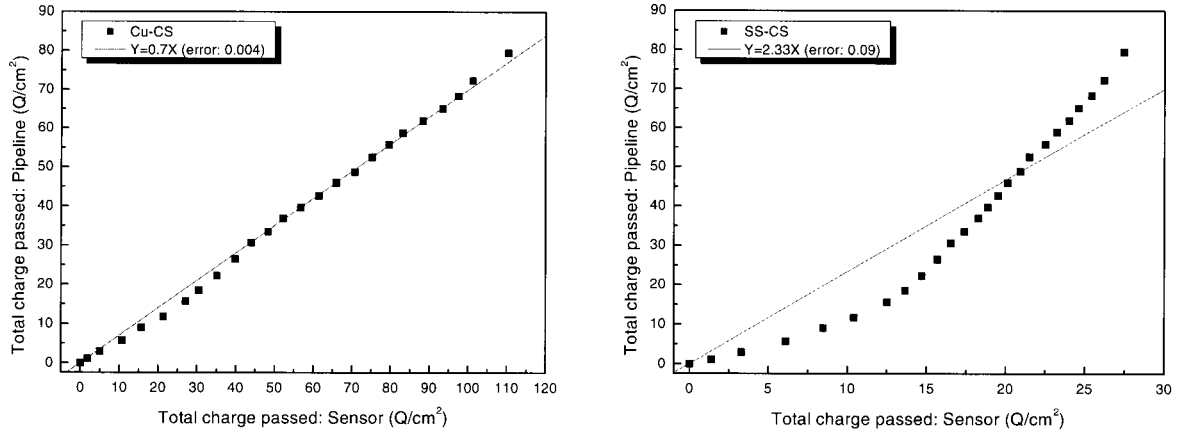

(a) (b)

Fig. 22. The relationship between the cumulative charges of pipeline steel obtained from LPR measurement and sensor output in synthetic tap water: (a) Cu-CS probe and (b) SS-CS probe.

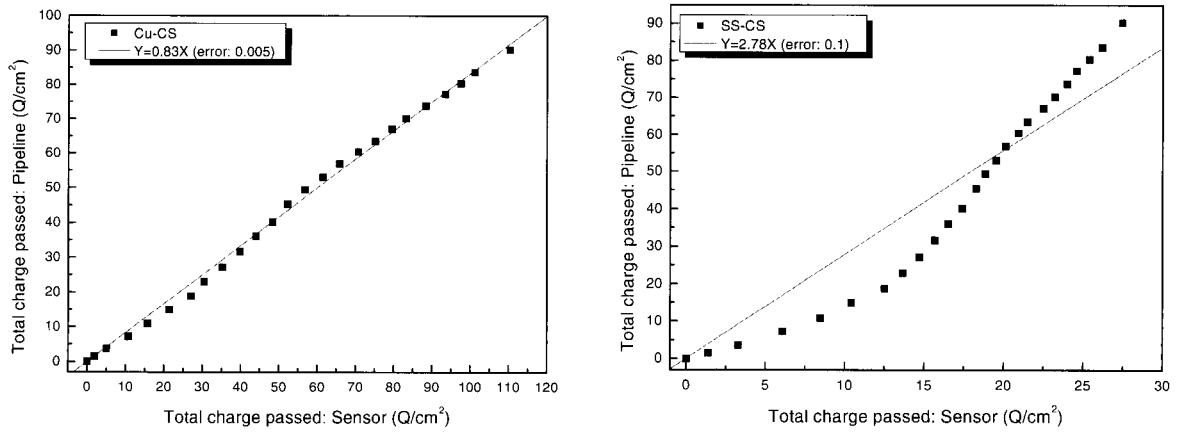

(a) (b)

Fig. 23. The relationship between the cumulative charges of pipeline steel obtained from EIS measurement and sensor output in synthetic tap water: (a) Cu-CS probe and (b) SS-CS probe.

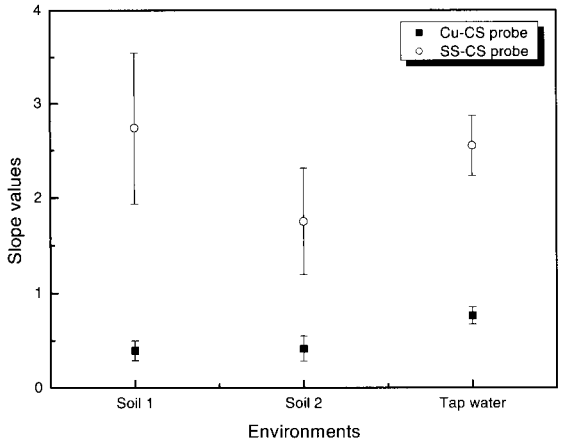

Fig. 24. Average slope parameters of the Cu-CS and SS-CS probes with different environments.

Tap water cell: Figs. 22 and 23 show the correlation between the coulomb values of the galvanic sensor and the pipeline steel obtained from LPR and EIS measurement in tap water cell. In synthetic tap water, only the Cu-CS probe shows a linear correlation between real corrosion rate of pipeline steel and sensor output. Thus, it can be also suggested that the Cu-CS sensor system has a possibility to predict the corrosion rate of pipeline steel in synthetic tap water.

According to the results of above investigation, it can be found that the sensor output of Cu-CS probe shows a good linear relationship with the corrosion rate of pipeline steel in soil and tap water environments. The definition of the slope parameter is expressed by the formula:

Slope = (Integrated Coulomb of the pipeline steel) / (Integrated Coulomb of the probe)

Based on the results from Figs. 18 ~ 23, the average slope parameters of the Cu-CS and SS-CS probes are shown in Fig. 24 with different environments. In the case of Cu-CS probe, the difference in slope parameters results from difference in the corrosivity of environment. The slope parameter of Cu-CS probe is 0.41 in soil cell 1, 0.39 in soil cell 2, and 0.76 in synthetic tap water, indicates that the slope parameter increases with increasing the corrosivity of environment. However, in the case of SS-CS probe, there is no correlation between slope parameter and environment.

4. Conclusions

1) The galvanic probe sensor evaluated herein exhibits good correlation to actual corrosion rate in soil and synthetic tap water environments. This indicated that the galvanic probe sensor system allows for the assessment of the moment of corrosion initiation and a quantitative determination of the external and internal corrosion rates of potable pipeline steel embedded in soil.

2) A good linear quantitative relationship was found between the Cu-CS probe current and the corrosion rate data of the pipeline steel coupons. Furthermore, the Cu-CS probe is more suitable for high resistance soil than SS-CS probe, due to the high current output.

3) A correlation based on the ratio of total charge passed obtained from the pipeline and the Cu-CS probe was determined as 0.4 in soil environments, and 0.76 in synthetic tap water, indicates that the slope parameter increases with increasing the corrosivity of environment.

4) However, several issues still remain to be solved in the practical application of this galvanic probe sensor system to structures in field, including data logger system, stray current, coating and cathodic protection. Some of these problems are currently underway to solve, and the system would be a valuable tool for continuous evaluation of the effectiveness of corrosion control methods at difficult accessible areas.

References

1. E.W. Klechka, *Mater. Perform.*, **41**, 24 (2002).
2. T.R. Jack and M.J. Wilmott, *Mater. Perform.*, **35**, 18 (1996).
3. A. Sander, B. Berghult, A.E. Broo, E.L. Johansson, and T. Hedberg, *Corros. Sci.*, **38**, 443 (1996).
4. A. Sander, B. Berghult, E. Ahlberg, A.E. Broo, E.L. Johansson, and T. Hedberg, *Corros. Sci.*, **39**, 77 (1997).
5. M.R. Schock, Water Quality and Treatment - A Handbook of Community Water Supplies, 4th ed., p.997, AWWA, McGraw-Hill, 1990.
6. A.W. Peabody, Control of Pipeline Corrosion, 2nd Ed., p.5, NACE, Houston, TX, 1967.
7. M.G. Fontana, Corrosion Engineering, 3rd Ed., p.383, McGraw-Hill, New York, NY, 1986.
8. V.S. Agarwala and S. Ahmad, "Corrosion Monitoring and Monitoring - A Review," *CORROSION/2000*, Paper No. 271, NACE, Houston, TX (2000).
9. Y. Miyata and S. Asakura, *Japan. Soc. Corr. Eng.*, **46**, 541 (1997).
10. D.L. Piron, R. Desjardins, F. Briere, and M. Ismael, "Corrosion Rate of Cast Iron and Copper Pipe by Drinkable Water," in Corrosion Monitoring in Industrial Plants Using Nondestructive Testing and Electrochemical Methods, ASTM STP 908, p.358, ASTM, Philadelphia, PA, (1986).
11. B. Elsener, M. Molina, and H. Bonhi, *Corros. Sci.*, **35**, 1563 (1993).

12. N.S. Berke, D.F. Shen, and K.M. Sundberg, "Comparison of Current Interruption and Electrochemical Impedance Techniques in the Determination of the Corrosion Rates of Steel in Concrete," *ASTM Sym. Ohmic Electrolyte Resistance Measurement and Compensation*, ASTM, West Conshohocken, PA (1988).
13. P.A. Cella and S.R. Taylor, *Corrosion*, **56**, 951 (2000).
14. NACE Publication 1C187, Use of Galvanic Probe Corrosion Monitors in Oil and Gas Drilling and Production Operations, NACE, Houston, TX (1995).
15. V.S. Agarwala, In-Situ Corrosivity Monitoring of Military Hardware Environments, *CORROSION/96*, Paper No.632, NACE, Houston, TX (1996).
16. M.D. Jaeger, B.R. Pilvelait, and P.J. Magari, Multilayer Galvanic Cell for Next Generation Corrosion Sensors, *CORROSION/2000*, Paper No. 302, NACE, Houston, TX (2000).
17. J. Gulikers, *Construction and Building Materials*, **11**, 143 (1997).
18. M. Raupach and P. Schiessl, *Construction and Building Materials*, **11**, 207 (1997).
19. M. Raupach and P. Schiessl, *NDT&E International*, **34**, 435 (2001).
20. J.P. Broomfield, K. Davies, and K. Hladky, *Cement & Concrete Composites*, **24**, 27 (2002).
21. T. J. Garosshen and T. K. Mukherji, On the Correlation of Bimetallic Corrosion Sensor Output to Actual Corrosion Damage, *CORROSION/2000*, Paper No. 266, NACE, Houston, TX (2000).
22. J.G. Kim, Y.W. Kim, and M.C. Kang, *Corrosion*, **58**, 175 (2002).
23. J.G. Kim and Y.W. Kim, *Corros. Sci.*, **43**, 2011 (2001).
24. S.W. Dean, Handbook on Corrosion Testing and Evaluation, John Wiley, New York, NY, p.171 (1971).
25. G.O. Davis, J. Kolts, and N. Sridhar, *Corrosion*, **42**, 329 (1986).
26. H.H. Uhlig, and R.W. Revie, Corrosion and Corrosion Control, 3rd Ed., p.29, John Wiley & Sons, New York, NY, 1985.
27. D.A. Jones, Principles and Prevention of Corrosion, 2nd Ed., p.168, Prentice-Hall, Upper Saddle River, NJ, 1996.
28. F. Mansfield and J.V. Kenkel, "Laboratory Studies of Galvanic Corrosion of Aluminum Alloys," in Galvanic and Pitting Corrosion- Field and Laboratory Studies, ASTM STP 576, p.20, ASTM, Philadelphia, PA1976.
29. J. C. Oung and H. C. Shih, *Corrosion Prevention & Control*, December, 173 (1997).
30. Y.S. Choi and J.G. Kim, *Corrosion*, **56**, 1202 (2000).